Splay and bend deformations in cells near corners

Supplemental materials

Aniruddh Murali, Prasoon Awasthi, Kirsten Endresen, Arkadiusz Goszczak and Francesca Serra

Supplemental Materials

Figures

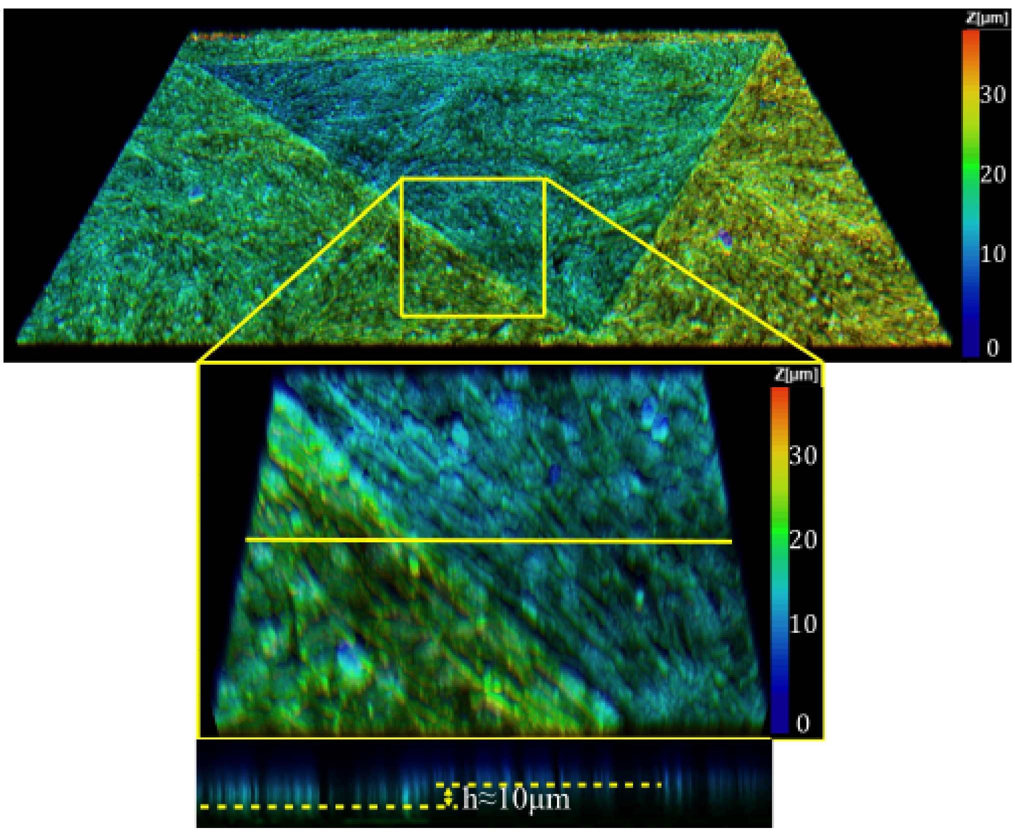

Figure S1: Confocal image of cells cultured on an equilateral triangle-patterned substrate. The image was captured from a fixed sample grown for 48 hours post-seeding. The sample is stained for actin (Rhodamine Phalloidin) and nuclei (DAPI). Each triangle edge measures 1800 μm. The z-scale bar is inverted. An enhanced view of the inset highlights the height variation between the patterned region and the substrate. A cross-section along the yellow line, color-coded to represent height variations, is also displayed.

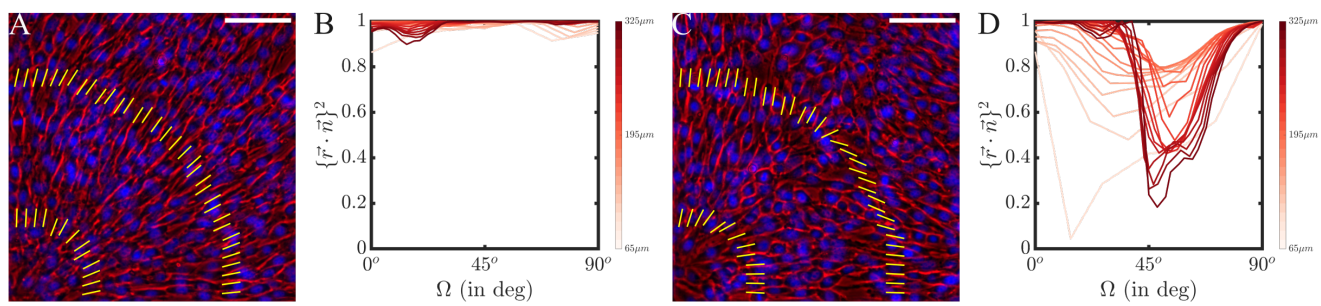

Figure S2: (A) Representative example of a splay deformation, with two orientations shown at radial distances of 130 μm and 325 μm for deformations observed at a 90° vertex, located at the lower left corner of each image. The red channel shows phase contrast imaging, while the blue channel displays fluorescence imaging of cell nuclei stained with NucBlue LiveCell Stain for enhanced visualization. (B) Plot of the function $\{\hat{r}\cdot\hat{n}\}^2$ vs. Ω for the splay deformation shown in A. (C) Example of an "imperfect´´ splay deformation at radial distances of 130 μm and 325 μm, also observed at a 90° vertex. (D) Plot of $\{\hat{r}\cdot\hat{n}\}^2$ vs. Ω for the deformation shown in C, which deviates from the expected splay trend but is still recognized as splay according to our categorization rule. (Scale Bar: 100 μm)

Wedge angle θ	Number of data points
1. $\pi/6$	7
2. $\pi/4$	28
3. $\pi/3$	79
4. $\pi/2$	21
5. $2\pi/3$	18
6. $5\pi/6$	16

Table 1: Statistics of different data points for various values of wedge angle (θ)

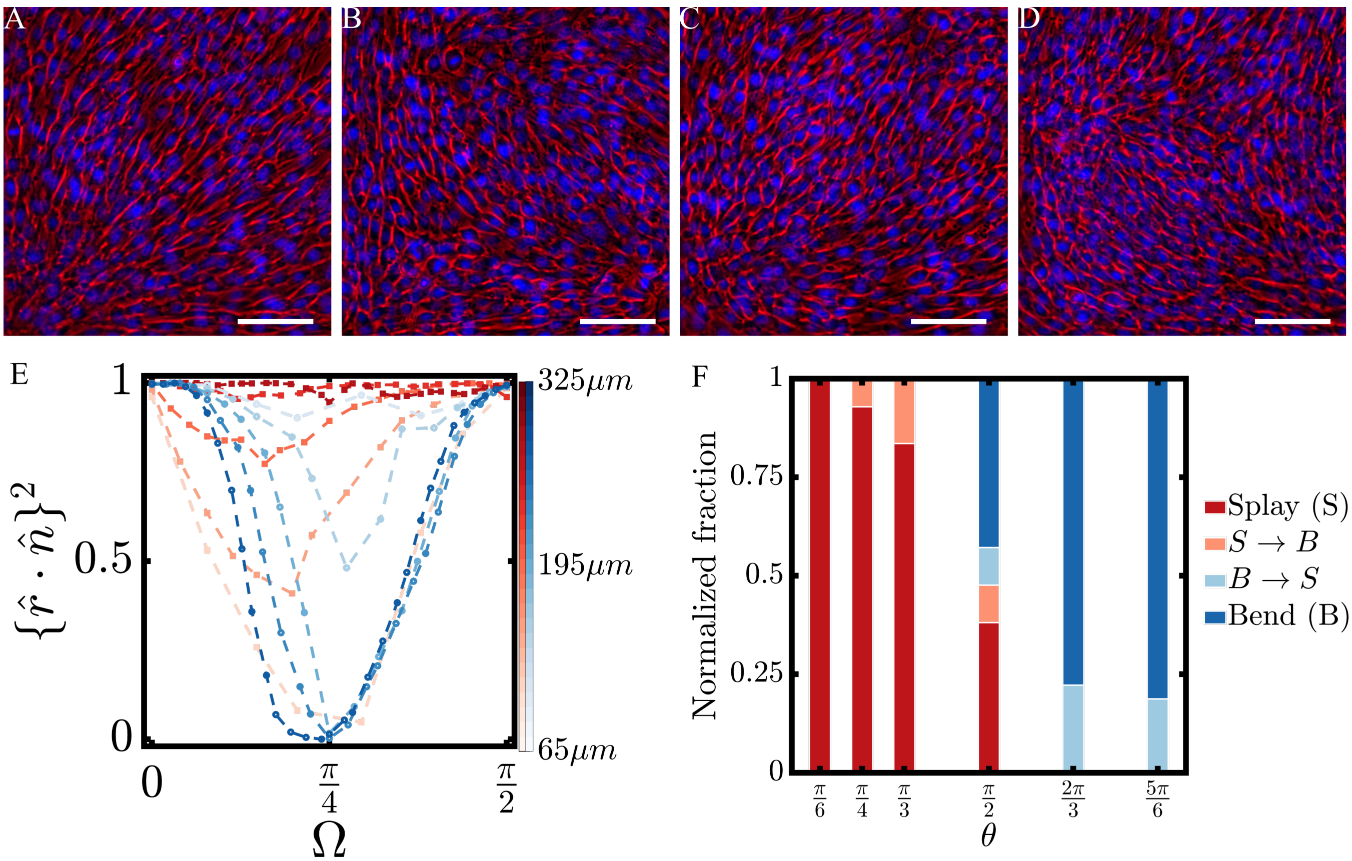

Figure S3: Example of (A) splay (B) splay-bend (C) bend-splay (D) bend deformation that is observed in the experiments at 90° vertex, positioned at the left bottom corner of each image. The red channel is the phase contrast imaging and the blue channel is the fluorescence imaging of cell nuclei stained with NucBlue LiveCell Stain for better visualization.(Scale Bar: 100 μm. (E)$\{\hat{r}\cdot\hat{n}\}^2$ vs Ω for two experimental cases with splay to bend (blue) and bend to splay (red) is observed. The color intensity goes from light to dark both transitions bend to splay (red) and splay to bend (blue) as the distance from the vertex is increased from 65μm to 325μm. (F) Fraction of observed splay and bend deformations as a function of the wedge angle θ (number of samples detailed in SI Table 1). Red columns are for pure splay deformation, light red for splay-to-bend transition, light blue for bend-to-splay and blue for pure bend deformation.

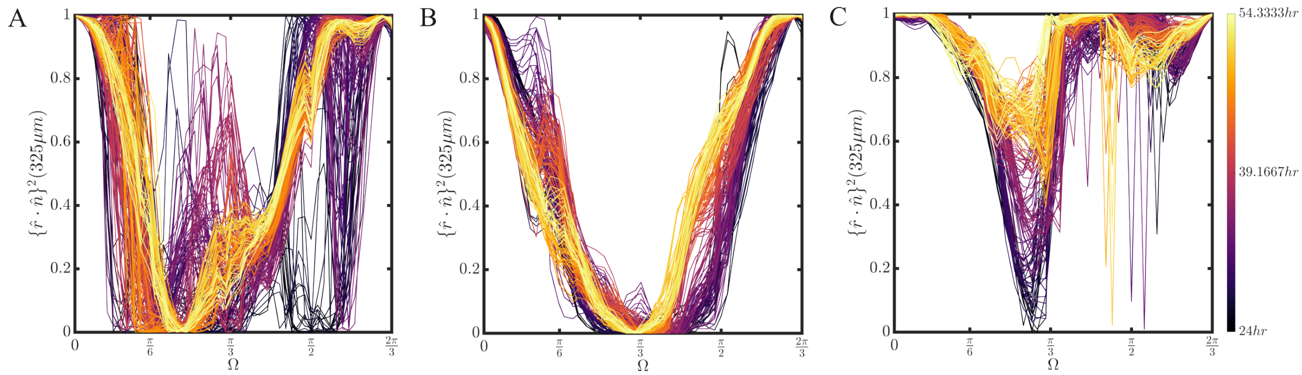

Figure S4: Representative plots of $\{\hat{r}\cdot\hat{n}\}^2$ versus Ω for deformations at $\theta = \frac{2\pi}{3}$, measured at a radial distance of 325 μm. The evolution over time from 24 to 54 hours is indicated by the color gradient. (A) Example showing bend-like deformations with significant noise at early timepoints. (B) Example with clear emergence of bend deformations from the beginning. (C) A less commonly observed splay configuration, appearing at higher density and accompanied by early-time noise.

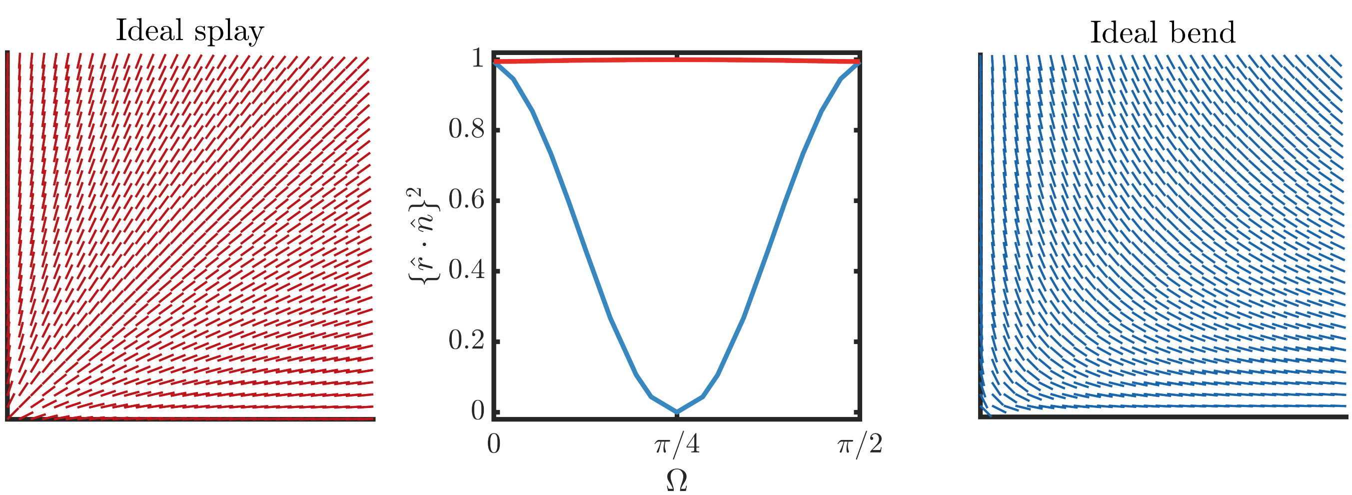

Figure S5: Reconstructions of Splay (left, red) and Bend (right, blue) director field near a corner with amplitude $\pi/2$ and planar alignment on the edges. The central panel shows the values of $(\hat{r}.\hat{n})^2$ for the two calculated director fields.

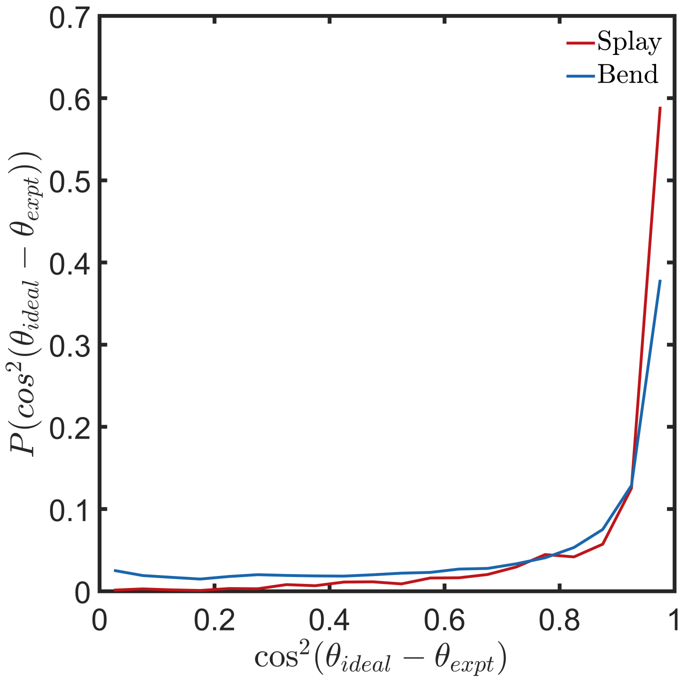

Figure S6: Measured difference between the calculated director field and the experimental observations. θ_{expt} is the orientation of the director averaged over different experimental realizations for a 90° wedge, for pure splay and pure bend case. θ_{ideal} is the theoretical director orientation for splay and bend deformation. In the figure the distribution of the difference between the experimental θ_{expt} and the theoretical θ_{ideal} for splay (red) and bend (blue) deformations is plotted as a function of the cosine square of $\theta_{ideal} - \theta_{expt}$

Experiments

Planar anchoring measurements

The orientation field was extracted using OrientationJ from phase contrast microscopy images. For each realization, data were recorded in a region extending 30 μm inward from each edge of the triangular confinement. Measurements were taken both across different alignment angles and, for selected cases, as a function of time. To quantify alignment relative to the boundary, the local orientation at each point was referenced to the corresponding edge orientation and normalized. As an example, for right angled triangle ($\theta = \frac{\pi}{2}$), the horizontal edge was defined as the zero-angle reference, and the orientation of points near the perpendicular edge was corrected by subtracting $\frac{\pi}{2}$. This results for images taken 48hr after is shown in the Fig.2C.

Theory

Splay and bend

In the Fig.2C in the main text the director field has strong planar anchoring with the edges of the triangle, and since the cells are arranged in a monolayer, the nematic director is confined to the xy plane. We can thus describe the nematic director as a function of the polar angle ϕ as $n_x = cos\,\phi$, $n_y = sin\,\phi$, and $n_z = 0$ from[1;2].

To describe the director orientation near the corners, we use the analytical form from[3]

$$\phi = s\alpha + c \tag{Eq.1}$$

where $\alpha = \tan^{-1}(y/x)$ and c is constant. The director field for the splay deformation, characterized by planar anchoring, can be conceptualized as a fraction of a +1 topological defect, with the angle going from 0 to θ (wedge angle). Therefore $s = 1$ and $c = 0$ as per reference[3]. By inserting these values into (Eq.1) and converting into cylindrical coordinates ϕ and r we get a director field given by (Eq.2) for splay deformation near a corner. For bend-like deformation, the liquid crystal molecules exhibit planar anchoring adjacent to the walls. The change occurs in between the walls, effectively shifting from radial alignment near the walls to azimuthal alignment in the middle. Therefore given the constraints we use the director orientation in (Eq.3).

$$\hat{n}_{splay} = \hat{r} + 0\hat{\phi} \tag{Eq.2}$$

$$\hat{n}_{bend} = cos\left(\frac{\pi}{\theta}\phi\right)\hat{r} - sin\left(\frac{\pi}{\theta}\phi\right)\hat{\phi} \tag{Eq.3}$$

The director is plotted in Fig.S5 where we see the theoretical directors of the splay and bend plotted along with the analysis of how the $(\hat{r}\cdot\hat{n})^2$ varies as a function of the angle Ω formed between the x-axis and the versor $\hat{r}$. We compare the director shown in Fig.S5 with the director measured experimentally and Fig.S6 shows that the difference is small for both bend and splay configurations.

Energy Calculation

The 3D Frank-Oseen energy is defined by (Eq.4),[1;2], where k_1, k_2, and k_3 denote the elastic constants for splay, twist, and bend, respectively, and $\hat{n}$ represents the director field. As the cell monolayer is restricted to xy plane the twist energy term (characterized by k_2) from the (Eq.4) can be discarded. Moreover the deformations can be considered only 2D, therefore both divergence and curl would be calculated only in 2D. This generates the free energy density per area in (Eq.5) where the elastic constants are given by k_1^* and k_3^* which are the 2D splay and bend elastic constants. For simplicity, from now on we call them k_1 and k_3 even if they are defined in 2D.

$$f_{FO} = \frac{1}{2}k_1(\nabla\cdot\hat{n})^2 + \frac{1}{2}k_2(\hat{n}\cdot\nabla\times\hat{n})^2 + \frac{1}{2}k_3(\hat{n}\times(\nabla\times\hat{n}))^2 \tag{Eq.4}$$

$$f_{FO_{2D}} = \frac{1}{2}k_1^*(\nabla\cdot\hat{n})^2 + \frac{1}{2}k_3^*(\hat{n}\times(\nabla\times\hat{n}))^2 \tag{Eq.5}$$

Integrating the Frank-Oseen energy over the wedge area and including the line anchoring term (analog to the surface anchoring energy) we get the total energy of the system as (Eq.6), where W is anchoring energy per unit length, l is the length of the wedge line, and $\hat{\tau}$ being the tangent vector to the edge.

$$E_{tot} = \int_0^l \int_0^\theta f_{FO}\, r\, d\phi\, dr - 2\int_0^l W(\hat{n}\cdot\hat{\tau})^2\, dl \tag{Eq.6}$$

As seen from Fig.2.C in the main text, the probability of cells aligning within 10 degrees of the wedge line is high for varying wedge angle. Thus we can imagine the contribution of the line anchoring energy to be zero. We know from (Eq.2) the functional form of $\hat{n}$ for splay deformation. If we assume the wedge angle to be θ and substitute it in (Eq.4) we get

$$f_{FO_{splay}} = \frac{1}{2}k_1\frac{1}{r^2} \tag{Eq.7}$$

because the bend term is zero. Substituting results of (Eq.7) in (Eq.6) we get the total energy for pure splay deformation as

$$\begin{aligned} E_{tot_{splay}} &= \int_\varepsilon^l \int_0^\theta \frac{1}{2}k_1\frac{1}{r^2}\, r\, d\phi\, dr \\ &= \int_\varepsilon^l \frac{1}{2}k_1\frac{1}{r}\,\theta\, dr + E_{cs} \\ &= \frac{1}{2}k_1\theta\, \ln\frac{l}{\varepsilon} + E_{cs} \end{aligned} \tag{Eq.8}$$

where ε is defect core, necessary to prevent the integral from diverging in zero and E_{cs} is the energy of the defect core. From (Eq.8) one can see that the energy for splay is a linear function of θ. One can do the same with the bend deformation case discussed before in (Eq.3) with $m = \frac{\pi}{\theta}$ and substitute in (Eq.4)

$$f_{FO_{bend}} = \frac{1}{2}k_1\frac{\cos^2 m\phi}{r^2}(1-m)^2 + \frac{1}{2}k_3\frac{\sin^2 m\phi}{r^2}(1-m)^2 \tag{Eq.9}$$

An important difference in this case as compared to the pure splay deformation is the presence of a component of energy coming from both splay and bend energy. Therefore the total energy from bend deformation is given by

$$\begin{aligned} E_{tot_{bend}} &= \int_\varepsilon^l \int_0^\theta \left[\frac{1}{2}k_1\frac{\cos^2 m\phi}{r^2}(1-m)^2 + \frac{1}{2}k_3\frac{\sin^2 m\phi}{r^2}(1-m)^2\right] r\, d\phi\, dr \\ &= \frac{1}{2}(1-m)^2\int_\varepsilon^l \left[k_1\frac{1}{r}\frac{\pi}{2m} + k_3\frac{1}{r}\frac{\pi}{2m}\right] dr + E_{cb} \\ &= \frac{(1-m)^2}{2}(k_1+k_3)\frac{\pi}{2m}\ln\frac{l}{\varepsilon} + E_{cb} \\ &= (1-\frac{\pi}{\theta})^2\frac{\theta}{4}(k_1+k_3)\ln\frac{l}{\varepsilon} + E_{cb} \end{aligned} \tag{Eq.10}$$

as $m = \pi/\theta$. Here E_{cb} represents the core energy of the bend defect, which we assume is small and equal to E_{cs}. It is of interest to note that the role of θ is not linear as seen with (Eq.8). We now have sufficient machinery to compare the two different deformations for the same angle.

Energy-Probability

The energy for the deformations are derived in (Eq.8), and (Eq.10) for splay and bend respectively. We have seen from the experimental results, that for the case of fibronectin coated cell substrate shown in Fig.2E in the main paper, the probability to splay or bend is equal for the case when $\theta = \frac{\pi}{2}$. This suggests that the energy associated to splay and bend is equal, thus allowing us to equate (Eq.8) and (Eq.10) at $\theta = \frac{\pi}{2}$

$$\begin{aligned} E_{splay} &= E_{bend} \quad \text{when} \quad \theta = \frac{\pi}{2} \\ \frac{k_1}{2}\frac{\pi}{2}\ln\frac{l}{\varepsilon} &= (1 - \frac{\pi}{\frac{\pi}{2}})^2 \frac{\pi}{2}\frac{(k_1 + k_3)}{4}\ln\frac{l}{\varepsilon} \\ k_1 &= k_3 \end{aligned} \tag{Eq.11}$$

Elastic Anisotropy

The above condition from (Eq.11) is valid for when the energy of splay and bend deformation are equal at $\theta = \frac{\pi}{2}$, what happens if that's not the case? We can still get the ratio between the elastic constants, using (Eq.8), and (Eq.10), and getting it as a function of θ_e, i.e. the arbitrary angle at which the two energy are the same.

$$\begin{aligned} E_{splay}(\theta_e) &= E_{bend}(\theta_e) \\ \frac{k_1}{2}\theta\ln\frac{l}{\varepsilon} &= (1 - \frac{\pi}{\theta})^2 \theta \frac{(k_1 + k_3)}{4}\ln\frac{l}{\varepsilon} \\ \frac{k_1}{k_3} &= \frac{(1 - \frac{\pi}{\theta})^2}{(1 - \frac{\pi^2}{\theta^2} + 2\frac{\pi}{\theta})} \end{aligned} \tag{Eq.12}$$

the plot for this function vs θ_e is shown in Fig.3C of the main paper.

References

[1] P. de Gennes and J. Prost, *The Physics of Liquid Crystals*, Clarendon Press, Oxford, 1993.

[2] M. Kleman and O. D. Lavrentovich, *Soft Matter Physics: An Introduction*, Springer New York, 2003.

[3] S. Chandrasekhar and G. S. Ranganath, *Advances in Physics*, 1986, **35**, 507–596.